

Reactions at Solid–Liquid Interfaces. The Mechanism and Kinetics of the Fluorination of 2,4-Dinitrochlorobenzene Using Solid Potassium Fluoride in Dimethylformamide

Gavin Macfie, Benjamin A. Brookes, and Richard G. Compton*

Physical and Theoretical Chemistry Laboratory, Oxford University, Oxford OX1 3QZ, U.K.

Received: July 11, 2001

The halogen exchange reaction of 2,4-dichloronitrobenzene with potassium fluoride in dimethylformamide containing tetrabutylammonium salts has been studied employing an electrochemical detection methodology based upon the use of square wave voltammetry to follow the loss of reactant and the formation of the product and intermediates. The results obtained show that the kinetics of loss of parent material behave on one hand as a dissolution-rate-controlled process and on the other as a homogeneous chemical process. Initially homogeneous reaction dominates the observed kinetics as the presaturated solution is stripped of fluoride ion; at longer time, the observed kinetics are controlled by the rate of KF dissolution. Modeling the system using a fully implicit finite difference method with Richtmyer modification (FIRM algorithm) yielded a mean value for the homogeneous rate constant for the formation of 2,4-dinitrofluorobenzene by reaction of 2,4-dichloronitrobenzene with fluoride ion in DMF at 85 °C of $640 \pm 250 \text{ mol}^{-1} \text{ cm}^3 \text{ s}^{-1}$ and a mean value for the saturation concentration of fluoride ion of $(6.5 \pm 0.5) \times 10^{-6} \text{ mol cm}^{-3}$. Ultrasound was found not to significantly enhance the rate of the reaction in the intensity range studied. Furthermore, the utility of microelectrodes for obtaining simple quantifiable voltammetric responses from compounds of which the macroelectrode responses are complicated by chemical followup steps is demonstrated. Ultrasonically induced mixing has been shown to facilitate reproducible microelectrode responses in intrinsically heterogeneous systems.

1. Introduction

Halogen exchange (HALEX) reactions, in which a chlorinated aromatic molecule undergoes substitution of chlorine for fluorine under phase-transfer catalysis (PTC) conditions, are widely used in many areas, including the pharmaceutical, agrochemical, and dyestuff industries.¹ Despite the wealth of fluorination agents that have been developed,¹ the use of alkali metal fluorides remains widespread with solid potassium fluoride (KF) giving the best compromise between cost and reactivity, CsF being both more reactive and more expensive and LiF and NaF being completely unreactive.² Considerable effort has been devoted to developing pretreatments that increase the area of KF available for reaction; these include spray-drying,³ freeze-drying,⁴ recrystallization from methanol,⁵ and the use of various materials including alumina⁶ and calcium fluoride⁷ as supports. Recently, polymers have also been used as supports for fluorinating agents.⁸ Tetraalkylammonium salts are commonly used as phase-transfer catalysts; however, tetrabutylammonium fluoride (TBAF) and tetramethylammonium fluoride (TMAF) are also effective in promoting fluorodenitration reactions, in which a nitro group undergoes substitution by fluoride.^{9,10}

One of the most extensively studied phase-transfer-catalyzed solid–liquid HALEX reactions is the chlorination of *n*-hexyl bromide by alkali metal chlorides in toluene with tetrabutylammonium bromide as the phase-transfer catalyst.^{11–13} It has been concluded that a ternary complex involving the solid ionophore, the alkyl halide, and the phase-transfer catalyst is fundamental to the mechanism.

SCHEME 1



Phase-transfer-catalyzed HALEX reactions of chlorinated nitrobenzenes are less-well-understood. The reaction of 2,4-dichloronitrobenzene (2,4-DCNB) in DMF under PTC conditions^{2,5,14} has been studied carefully by several authors, but nevertheless, the mechanism of the reaction remains open. In particular, two mechanistic variations can be envisaged. First, the organic molecule reacts at the solid surface^{2,5} in a truly interfacial manner. Second, the KF may dissolve and the fluorination take place homogeneously. Within the second limit, two further possibilities exist as to whether the dissolution or the homogeneous reaction is rate-limiting.

This complete mechanistic uncertainty prompted us to study the HALEX reaction of a chloronitrobenzene with solid KF under PTC conditions (Scheme 1). Specifically, the reaction of 2,4-dinitrochlorobenzene (2,4-DNCB) with potassium fluoride in dimethylformamide was selected for study. Because of the mesomeric effect of the para nitro group in the plane of the aromatic ring, this substrate is much more activated to nucleophilic aromatic substitution than 2,4-DCNB, in which the mesomeric effect of the nitro group is mitigated by the steric effects of an ortho chlorine. Hence, relatively low temperatures can be used to study the reaction. The product of this fluorination reaction, 2,4-dinitrofluorobenzene (2,4-DNFB), is known as Sanger's reagent and has long been used as a reagent for labeling terminal amino acid groups.¹⁵

* To whom correspondence should be addressed. Tel: 0044(0)-186527540. Fax: 0044(0)1865275410. E-mail: richard.compton@chemistry.ox.ac.uk.

Previous kinetic investigations of HALEX reactions have relied upon analyzing samples withdrawn from the reaction vessel by methods such as gas chromatography. However, we have employed a unique real-time electrochemical detection methodology based upon the use of square wave voltammetry,¹⁶ a versatile electrochemical technique, which gives a peaked response. The deconvolution of the responses due to all of the voltammetrically visible components allows the evolution in time of each of their concentrations so permits clear and unambiguous mechanistic insight. The results presented show that the kinetics of the HALEX reaction studied are mixed, the site of reaction being in solution but the reaction occurring at a rate influenced by the kinetics of fluoride dissolution. The application of microelectrode techniques is fundamental to the method because, by virtue of their reduced diffusional time scale, they may outrun the kinetics of any chemical step following electrochemical transformation. Purely electrochemical current responses are thus obtainable. Chemical processes following the electrochemical step may complicate the observed current response at a macroelectrode. In heterogeneous systems, it has been shown that microelectrode responses reflect the concentrations of solution species local to the electrode.^{17–20} These local concentrations may differ significantly from the bulk concentrations in the same system. We demonstrate that ultrasonically induced mixing facilitates the measurement of a microelectrode response that accurately reflects bulk concentration in the intrinsically heterogeneous system studied.

That ultrasound can enhance the rate of solid–liquid heterogeneous reactions operating under conditions of phase-transfer catalysis is well-known;²¹ examples include *N*-alkylation of amines in water,²² synthesis of benzyl sulfide from benzyl chloride and sodium sulfide in nonaqueous solvents,²³ and the Michael reaction of ethyl malonate to chalcone in toluene.²⁴ The chemical effects of ultrasound are generally seen in single electron-transfer reactions involving the formation free radicals;²⁵ however, where an ionic mechanism is followed, ultrasonically induced rate enhancements are generally due to mechanical effects, most notably increased mass transport across the solid–liquid interface through a diffusion layer thinned by acoustic streaming effects.²⁵ Cavitation effects can also influence rate in solid–liquid systems through several mechanisms: microstreaming of solvent jets can lead to fragmentation of solid particles, increasing the area available for reaction;² products and intermediates can be swept away rapidly from the solid surface, thus renewing the surface for reaction.²⁵

2. Experimental Section

Tetrabutylammonium tetrafluoroborate (TBABF₄, purum, H₂O < 2%), decamethyl ferrocene (dmFc), and *N,N*-dimethylformamide (DMF, puriss., H₂O ≤ 0.01%) were obtained from Fluka. Spray-dried potassium fluoride (KF), 2,4-dinitrochlorobenzene (2,4-DNCB, 99+%,), and 2,4-dinitrofluorobenzene (2,4-DNFB, 99%) were obtained from Aldrich. All materials were used as supplied with the exception of KF, which was oven-dried at 120 °C for 2 h at atmospheric pressure.

Voltammetry was performed using an Autolab computer-controlled PGSTAT 20 potentiostat (Ecochemie, Utrecht, Netherlands). Platinum disk electrodes of diameter 7 mm and 25 μm were used for the preliminary voltammetry, while kinetic measurements were performed using only the 25 μm platinum disk. Working electrodes were polished sequentially with aqueous slurries of alumina of particle size 3.0, 1.0, and 0.3 μm (Kemet) prior to use.²⁶ Rotating disk measurements were carried out using a standard rotating disk electrode rotator

(Oxford Instruments, Oxford, U.K.). In all experiments, the counter electrode was a Pt coil and the reference electrode was a Ag wire pseudoreference. All three electrodes were immersed directly into the solution being studied.

Power ultrasound of frequency 20 kHz was provided by a Heat Systems Ultrasonics (Farmingdale, NY) W-380 ultrasonic horn of diameter 13 mm. The horn tip was insulated via a polytetrafluoroethylene ring and a Delrin screw connection. The power output of the transducer has been calorimetrically calibrated for each experimental configuration.²⁷

The procedure used to gather kinetic data was as follows. A five-necked 100 mL flask was oven-dried at 150 °C and cooled under an argon (Pureshield, BOC) purge. The counter and pseudoreference electrodes were fitted to the flask. The supporting electrolyte (TBABF₄) and KF were then added prior to introduction of 50 mL of DMF through transfer lines under nitrogen pressure. The solution was then degassed for 10 min with argon. Upon conclusion of degassing the solution, the ultrasonic horn was inserted through the central fifth neck; Parafilm was used to seal the neck, while a flow of argon over the solution ensured that no oxygen contacted the solution. The solution was sonicated using an ultrasound power of 50 W cm⁻² for 10 min to “activate” the KF. Sonication using intensities between 20 and 200 W cm⁻² has been shown to reduce the average particle size² of spray-dried KF from 100 to 30 μm.

Temperature control was most important, and care was taken to ensure that all experiments were carried out at 85 ± 1 °C. Three regimes were studied; in the first, in which magnetic stirring was used to maintain the KF in suspension, water heated to 85 ± 1 °C was circulated by pump from a waterbath to a plastic beaker surrounding the cell. The two other regimes, in which ultrasound intensities of 25 and 50 W cm⁻² were employed, required circulation of water at 76 and 65 °C, respectively, to maintain the solution temperature at 85 ± 1 °C.

Once the solution temperature had stabilized in the presence of the required stirring or ultrasonic agitation, a platinum microdisk electrode was inserted and 1 mL of a freshly prepared stock solution of 2,4-DNCB in DMF was charged using an Eppendorf pipet to give a final concentration of 10 mM. Simultaneously with the DNCB addition a data acquisition program was initiated to gather square wave voltammetry (SWV) traces at predetermined intervals for the duration of the experiment. The SWV data were analyzed using the nonlinear curve fitting function of Microcal Origin (Microcal Software Inc., Northampton, MA) to yield reaction profiles. The composite experimental traces were fitted using a simplex²⁸ routine to fit multiple Gaussian peaks of known width at half-height and peak-to-peak separation.

The information gained from the deconvolution of the SWV data was complemented by UV–vis absorption spectra recorded using a Unicam UV2 Series UV–vis spectrophotometer (Unicam, Cambridge, U.K.). Samples for analysis were withdrawn from the reaction mixture, cooled to room temperature, and diluted by a factor of 100 with DMF containing 0.1 M TBABF₄ prior to measurement in a quartz cell of path length 1.0 cm. A background of DMF containing 0.1 M TBABF₄ was employed. Care was taken not to include any KF particles in the aliquot.

3. Results

3.1. Preliminary Voltammetry. The electrochemical behaviors of the starting material, 2,4-DNCB, and product, 2,4-DNFB, of the HALEX reaction were investigated at 25 ± 1 °C to select a voltammetric technique capable of providing a reliable

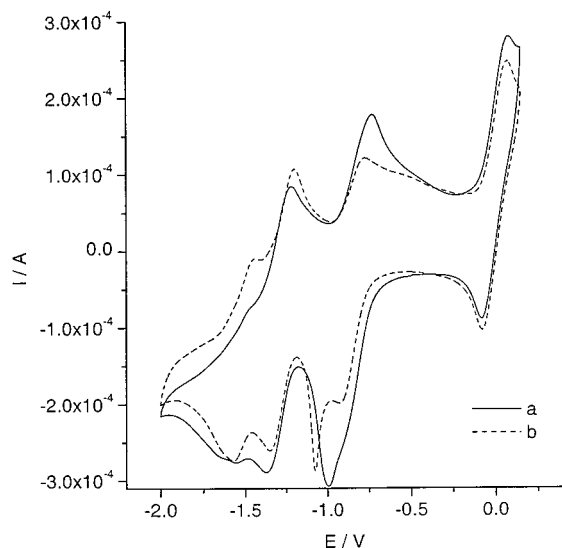


Figure 1. Cyclic voltammograms of 1.16 mM 2,4-DNCB with respect to 0.97 mM dmFc (a) and 1.25 mM 2,4-DNFB with respect to 0.98 mM dmFc (b) in DMF/0.1 M TBABF₄ recorded at a 7 mm diameter Pt disk with a Pt coil counter electrode and a Ag pseudoreference electrode at 25 °C.

measurement of their solution concentrations. Solutions in the concentration range of 1–10 mM of 2,4-DNCB or 2,4-DNFB were prepared in DMF/0.1 M TBABF₄ with or without the addition of 1 mM dmFc. The latter served to “calibrate” the pseudoreference electrode employed. First-scan cyclic voltammograms were recorded using a voltage scan rate of 500 mV s⁻¹ in the potential range of +0.2 to -2.0 V vs Ag at a 7 mm diameter Pt disk electrode. Steady-state cyclic voltammograms, obtained after the first scan, were then measured using voltage scan rates of 5–500 mV s⁻¹ in the potential range of +0.2 to -1.2 V vs Ag at a 7 mm diameter Pt disk electrode. Cyclic voltammograms were then registered at a 25 μm Pt microelectrode using potential scan rates in the range of 200–0.5 V s⁻¹. Additionally, steady-state voltammograms were measured at a 25 μm Pt microelectrode using a potential scan rate of 10 mV s⁻¹.

The macroelectrode voltammograms (Figure 1) resulting from potential scans in the range of +0.2 to -2.0 V vs Ag showed significant complexity, showing two consecutive reduction and oxidation waves but with additional peaks. 2,4-DNCB gave reduction peaks at -0.89 (shoulder), -0.99, -1.37, -1.52, and -1.69 V and oxidation peaks at -1.49 (shoulder), -1.22, and -0.73 V vs Ag pseudoreference. 2,4-DNFB exhibited reduction peaks at -0.93, -1.08, -1.35, and -1.57 V and oxidation peaks at -1.44, -1.20, and -0.78 V vs Ag pseudoreference. In both cases, dmFc gave a reduction peak at -0.06 V and an oxidation peak at +0.02 V. The voltammograms resulting from potential scans in the range of +0.2 to -1.2 V vs Ag featured only the first reduction wave for both 2,4-DNCB and 2,4-DNFB (Figures 2 and 3). The ratio of the forward and backward peaks for both compounds was found to increase with decreasing scan rate. The microelectrode voltammograms (Figures 4 and 5), however, exhibited forward and backward peak height ratios equal to 1.00 ± 0.05, indicating the formation of a stable radical anion capable of undergoing complete reoxidation to the parent. A steady-state response was observed at low scan rates indicating that the lower time scale of diffusion outruns the kinetics of the followup reaction, which caused an increase in the height of the first reduction waves in the corresponding macroelectrode experiments. The half-wave potentials of 2,4-DNCB and 2,4-DNFB in DMF/0.1 M TBABF₄ were determined to be -0.77

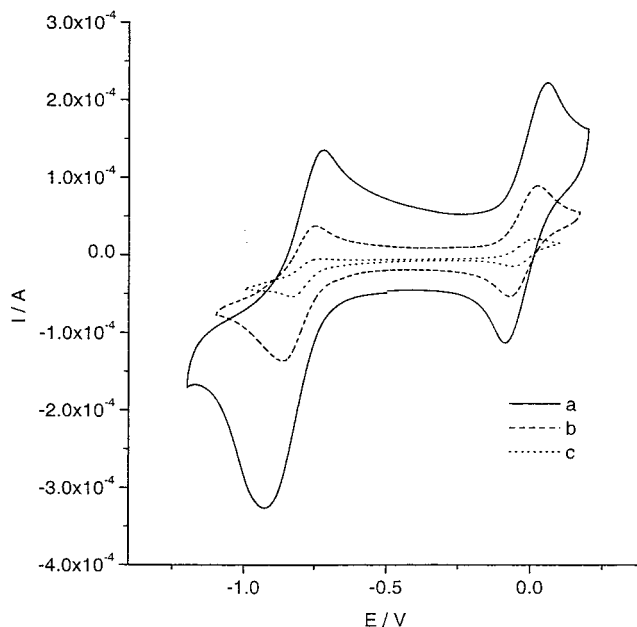


Figure 2. Cyclic voltammograms of 1.16 mM 2,4-DNCB with respect to 0.97 mM dmFc in DMF/0.1 M TBABF₄ recorded at a 7 mm diameter Pt disk with a Pt coil counter electrode and a Ag pseudoreference electrode at 25 °C: potential scan rates 500 (a); 50 (b); 5 mV s⁻¹ (c).

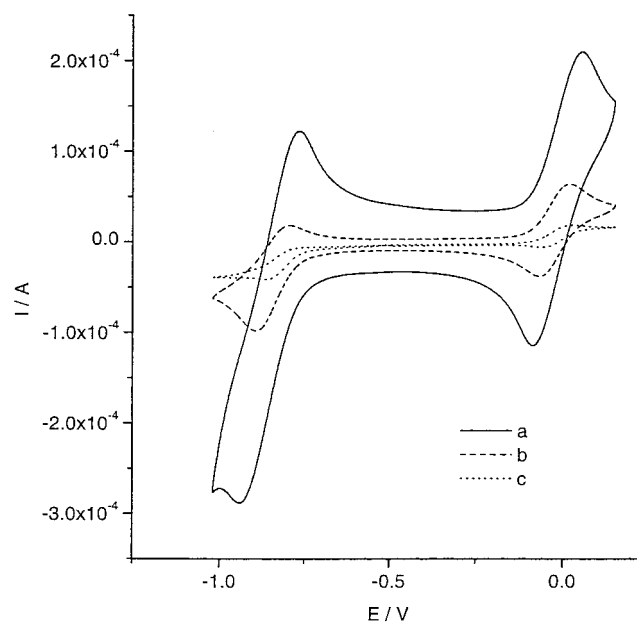


Figure 3. Cyclic voltammograms of 1.25 mM 2,4-DNFB with respect to 0.98 mM dmFc in DMF/0.1 M TBABF₄ recorded at a 7 mm diameter Pt disk with a Pt coil counter electrode and a Ag pseudoreference electrode at 25 °C: potential scan rates 500 (a); 50 (b); 5 mV s⁻¹ (c).

and -0.83 V vs the dmFc|dmFc⁺ redox couple, respectively, at 25 ± 1 °C.

The electrochemical behavior of 2,4-DNCB and 2,4-DNFB in DMF/0.1 M TBABF₄ has recently been investigated²⁹ and shown to be mechanistically complex. At voltage scan rates above 20 V s⁻¹, 2,4-DNCB exhibited behavior analogous to that of 1,3-dinitrobenzene, that of two consecutive reversible one-electron reductions with half-wave potentials of -0.88 and -1.34 V vs SCE indicating formation of a stable radical dianion. Below 20 V s⁻¹, new reduction peaks at -1.51 and -1.63 V vs SCE and a new oxidation peak at +0.68 V vs SCE were observed. Additionally, the height of the first wave was found to increase to more than one electron per mole. The authors

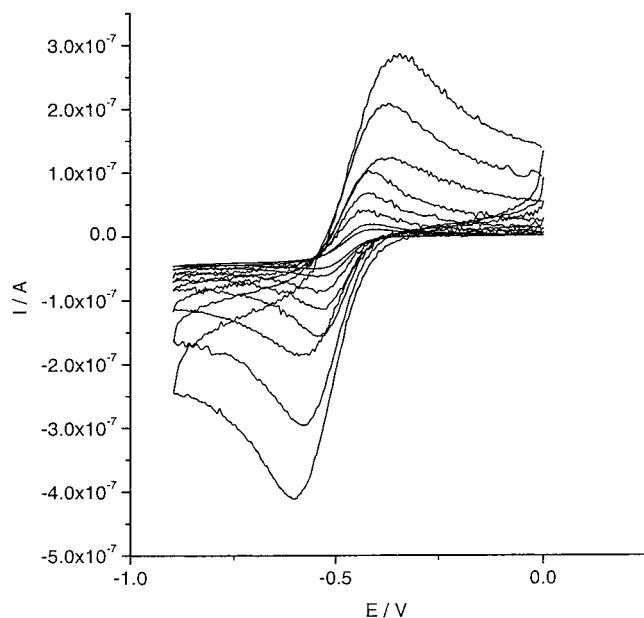


Figure 4. Cyclic voltammograms of 10.08 mM 2,4-DNCB in DMF/0.1 M TBABF₄ recorded at a 25 μ m diameter Pt disk with a Pt coil counter electrode and a Ag pseudoreference electrode at 25 $^{\circ}$ C at potential scan rates of 150–0.5 V s⁻¹.

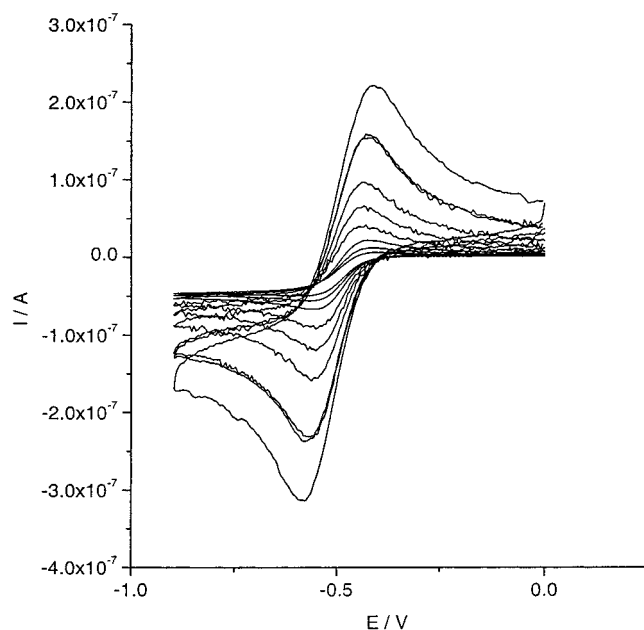


Figure 5. Cyclic voltammograms of 10.02 mM 2,4-DNFB in DMF/0.1 M TBABF₄ recorded at a 25 μ m diameter Pt disk with a Pt coil counter electrode and a Ag pseudoreference electrode at 25 $^{\circ}$ C at potential scan rates of 200–0.5 V s⁻¹.

attributed the new reduction peaks to the reduction of 2,2',4,4'-tetranitrophenyl (TNBP) formed through dimerization of the 1,3-dinitrobenzene radical that results from cleavage of the chlorine from 2,4-DNCB. Addition of water to the solution prevented the appearance of the TNBP peaks, indicating that hydrogen abstraction is the preferred pathway for the 1,3-dinitrobenzene radical, TNBP being formed only after all of the protons in the solution have been consumed. The electrochemical behavior of 2,4-DNFB was also found to depend on voltage scan rate with two consecutive reversible one-electron reductions indicating formation of a stable radical dianion. At scan rates less than 1 V s⁻¹, two additional reduction peaks were observed at -1.35 and -1.56 V vs SCE, an additional

oxidation peak was observed at +0.71 V vs SCE, and the height of the first reduction wave was found to increase. In this case, the explanation involves dimerization of the radical anion from the first reduction wave to form a Meisenheimer complex, which is reduced at -0.87 and -1.06 V vs SCE; this explains the increase in the first reduction wave. At potentials corresponding to the second wave, the reduction wave for the undimerized 2,4-DNFB radical anion and two small reduction waves resulting from two successive one-electron reductions from the product formed by the loss of the fluoride anions from the doubly reduced Meisenheimer complex were observed.

Excellent agreement exists between the data presented here and that presented by Gallardo et al., noting that the reference electrode employed in the latter study was an SCE, whereas a Ag wire pseudoreference was used in this work. In the case of 2,4-DNCB, Gallardo found peaks corresponding to the first and second reduction waves at -0.94 and -1.34 V and peaks corresponding to the reduction of TNBP at -1.41 and -1.63 V; this current study found peaks corresponding to the first and second reduction waves at -0.99 and -1.37 V and peaks corresponding to the reduction of TNBP at -1.52 and -1.69 V; the presence of the additional shoulder at -0.87 V, which does not appear in the former study, can be accounted for by the fact that it is steady-state data rather than first-scan data and as such will contain some 1,3-dinitrobenzene, the reduction potential of which is given in ref 29 as -0.82 V. In the case of 2,4-DNFB, Gallardo found peaks corresponding to the first reduction wave at -0.79, peaks corresponding to the reduction of the Meisenheimer complex at -0.87 and -1.06 V, and peaks corresponding to the reduction of the singly and doubly defluorinated Meisenheimer complex at -1.35 and -1.56 V. This current study found a peak corresponding to a composite of the first reduction wave of 2,4-DNFB and the first reduction wave of the Meisenheimer complex at -0.93 V, a peak corresponding to the second reduction waves of the Meisenheimer complex at -1.08, and peaks corresponding to the reduction of the singly and doubly defluorinated Meisenheimer complex at -1.35 and -1.57 V.

Last and importantly, comparison of the microelectrode data presented in this current study with the macroelectrode data presented in ref 29 demonstrates the utility of microelectrode techniques for the voltammetric study of systems in which chemical reaction follows an electrochemical step, because the shorter time scale of the experiment ensures that the electrochemical transformation can be reversed prior to the chemical step at lower scan rates than in the corresponding macroelectrode experiment. Thus, purely electrochemical voltammetric responses can be obtained in the case of both 2,4-DNCB and 2,4-DNFB by limiting the potential scan range and employing microelectrode techniques.

3.2. Determination of Diffusion Coefficients. Diffusion coefficients were first determined with microelectrode³⁰ techniques and subsequently confirmed by rotating disk methods. From solutions of 2,4-DNCB and 2,4-DNFB with concentrations of 10.02 and 10.25 mM, respectively, linear sweep voltammograms were recorded at a 12.5 μ m Pt disk electrode using a potential scan rate of 10 mV s⁻¹. The steady-state limiting currents thus obtained are presented in Figure 6 and were treated using the equation for the diffusion-limited current at a microelectrode¹⁶

$$I_{\text{lim}} = 4nFrDc_{\text{bulk}} \quad (3.1)$$

to obtain diffusion coefficients. In the above equation I_{lim} is the limiting current, n is the number of electrons transferred, F

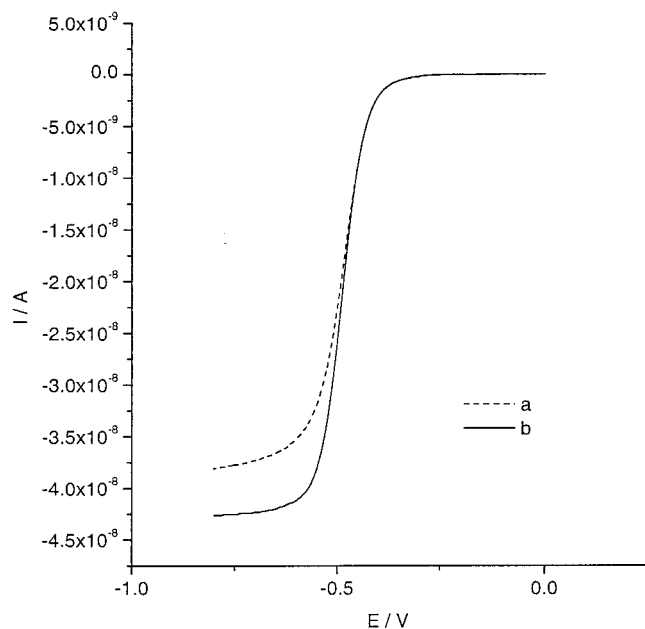


Figure 6. Steady-state microelectrode voltammograms of 10.02 mM 2,4-DNCB (a) and 10.25 mM 2,4-DNFB (b) in DMF/0.1 M TBABF₄ recorded on a 25 μm diameter Pt disk with a Pt coil counter electrode and a Ag pseudoreference electrode at 25 $^{\circ}\text{C}$ at a potential scan rate of 10 mV s^{-1} .

is the Faraday constant, r is the electrode radius, D is the diffusion coefficient, and c_{bulk} is the bulk concentration. To ensure accuracy, the area of the electrode was determined electrochemically with a compound of known diffusion coefficient. The diffusion coefficients of both 2,4-DNCB and 2,4-DNFB were thus measured to be $(0.9 \pm 0.1) \times 10^{-5} \text{ cm}^2 \text{ s}^{-1}$ at $25 \pm 1 \text{ }^{\circ}\text{C}$.

To confirm these measurements, solutions of 2,4-DNCB and 2,4-DNFB with concentrations of 1.16 and 1.25 mM, respectively, were prepared, and steady-state hydrodynamic voltammograms were recorded at a 7 mm Pt disk electrode rotating at frequencies between 1 and 36 Hz. A voltage scan rate of 50 mV s^{-1} was used. The limiting currents thus obtained were analyzed using the Levich equation for a rotating disk electrode³¹

$$I_{\text{lim}} = 0.62nFAc_{\text{bulk}}D^{2/3}\nu^{-1/6}\omega^{1/2} \quad (3.2)$$

to obtain diffusion coefficients. In the above equation, I_{lim} is the limiting current, n is the number of electrons transferred, F is the Faraday constant, A is the electrode area, c_{bulk} is the bulk concentration, D is the diffusion coefficient, ν is the kinematic viscosity of the solvent, and ω is the frequency of rotation. In the case of 2,4-DNFB, a straight-line limiting current vs (frequency)^{1/2} plot was obtained; from this, a value of $(0.9 \pm 0.1) \times 10^{-5} \text{ cm}^2 \text{ s}^{-1}$ was inferred for the diffusion coefficient. In the case of 2,4-DNCB, the limiting current vs (frequency)^{1/2} plot showed deviation from linearity at low frequencies, indicating a coupled chemical step implicated in measurements at the macroelectrode, and this precluded any inference of the diffusion coefficient.

The two independent measures of the diffusion coefficient of 2,4-DNFB are in excellent agreement. The value obtained for the diffusion coefficient of 2,4-DNCB by the microelectrode method is in excellent agreement with that calculated using the Wilke–Chang equation,³² $(1.0 \pm 0.1) \times 10^{-5} \text{ cm}^2 \text{ s}^{-1}$.

3.3. Square Wave Voltammetry. Square wave voltammetry (SWV) was used to obtain a peaked voltammetric response for both 2,4-DNCB and 2,4-DNFB in the potential range of 0 to

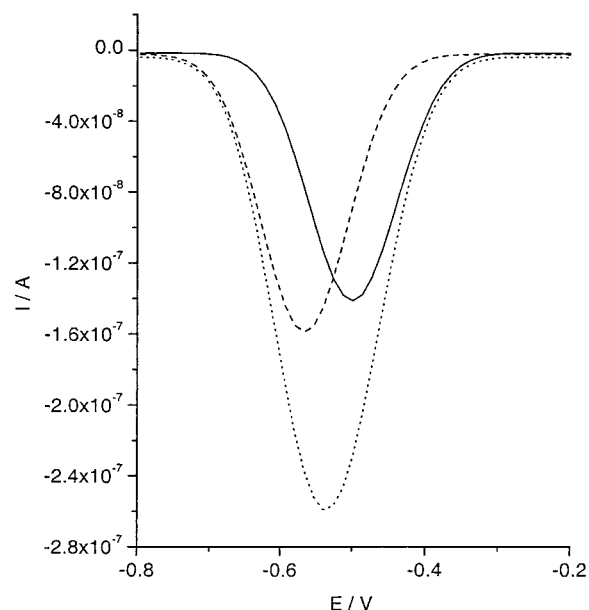


Figure 7. Square wave voltammograms for 9.33 mM 2,4-DNCB in DMF/0.1 M TBABF₄ (solid), composite signal obtained after addition of 2,4-DNFB to give a concentration of 10.24 mM (dots), and 2,4-DNFB signal obtained by subtracting the 2,4-DNCB signal from the composite (dashes) recorded at a 25 μm diameter Pt disk with a Pt coil counter electrode and a Ag pseudoreference electrode at 88 $^{\circ}\text{C}$: square wave amplitude 50 mV; frequency 50 Hz; step potential 5 mV.

–0.8 V vs Ag, the range in which the first reduction takes place for both compounds without any electrode deactivation. Both the resolution and the sensitivity are greatly enhanced in SWV with respect to dc methods.³³ A solution of 9.33 mM 2,4-DNCB was prepared in DMF/0.1 M TBABF₄ and heated to 88 $^{\circ}\text{C}$ with ultrasound. SWV traces were recorded at a 12.5 μm Pt disk electrode. The SWV pulse used had an amplitude of 50 mV, a step potential of 5 mV, and a frequency of 50 Hz. A quantity of pure 2,4-DNFB was then added by Eppendorf pipet to give a solution concentration of 10.24 mM, and SWV traces were recorded using the parameters detailed above. The 2,4-DNCB signal was subtracted to give the contribution of 2,4-DNFB to the mixture.

The results are presented in Figure 7; the peaks are substantially overlaid, but when the individual component peaks are resolved by subtracting the 2,4-DNCB signal from the composite signal obtained after 2,4-DNFB addition, it can be seen that both compounds give symmetrical, well-defined peaks. The position of the 2,4-DNCB peak is –0.505 V vs Ag and that of 2,4-DNFB is –0.560 V, giving a peak-to-peak separation of 65 mV. Curve-fitting shows that at $88 \pm 1 \text{ }^{\circ}\text{C}$ both peaks have a width at half-height ($W_{1/2}$) of 0.125 V.

3.4. Reaction Profiling via Square Wave Voltammetry.

In systems containing both 2,4-DNCB and KF in which the HALEX fluorination was occurring, a large number of SWV traces were gathered over the course of 2 h according to the procedure outlined in the Experimental Section. Experiments were carried out at 85 $^{\circ}\text{C}$ first in insonated conditions, in which the KF was kept in suspension by ultrasound of intensity 25 W cm^{-2} . At the start of each experiment, immediately after the addition of the 2,4-DNCB stock solution, the voltammetric response was that of the starting material, 2,4-DNCB. As time progressed, the peak reduced in height while broadening at the negative side. As the reaction progressed further, broadening was also observed at the positive side of the parent peak. A further effect, which occurred at longer time, was the appearance of a peak at more negative potential than the parent or the 2,4-

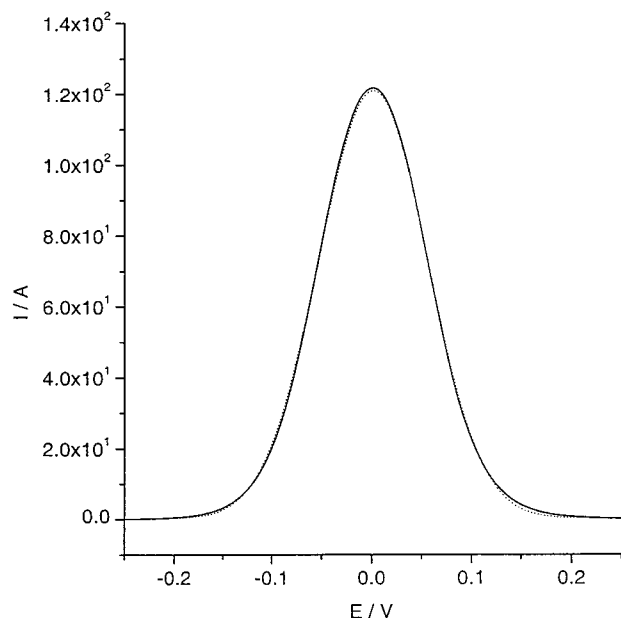


Figure 8. Fitting of a square wave voltammogram simulated according to the procedure in ref 34 (dots) with a Gaussian peak (solid): $R^2 = 0.99981$.

DNFB peak. The appearance of this peak was accompanied by a reduction in the height of the composite peak comprising the voltammetric responses of the parent, 2,4-DNFB, and the third peak. These processes are illustrated in Figure 9.

The data thus obtained were analyzed by deconvolution to resolve the contributions of the individual components, allowing the generation of reaction profiles. Four experiments were carried out in which the amount of KF added was increased from 1 to 8 g. This approach was then applied to a more intensely sonicated system employing ultrasound at 50 W cm^{-2} and finally to a “silent” system in which the KF was kept in suspension by mechanical agitation provided by a magnetic stirrer bar.

3.4.1. Characteristics and Modeling of the SWV Response and Reaction Profiles. We next consider the evolution of the SWV response at a typical HALEX reaction. At the start of each experiment, immediately after the addition of the 2,4-DNCB stock solution, the voltammetric response was that of the starting material, 2,4-DNCB and the data approximated to a high degree of accuracy with a single Gaussian peak of $W_{1/2} = 0.125 \text{ V}$. Figure 8 shows a SWV peak simulated according to the procedure detailed in ref 34 and the corresponding Gaussian fit ($R^2 = 0.99981$). As time progressed, the peak reduced in height while broadening at the negative side, indicating that the 2,4-DNCB initially present was being converted into another species with a more negative reduction potential. It was found that the best fit was obtained with two peaks of $W_{1/2} = 0.125 \text{ V}$ separated by 65 mV.

As the reaction progressed further, the experimental SWV response could no longer be fitted with these two peaks and the addition of a further peak, this time positive in potential from the parent compound, was required to obtain a good fit. Because the peak width of a Nernstian SWV peak is determined only by the amplitude of the square wave and the temperature,³⁵ a new peak also of width 0.125 V was required. Initially, the potential of this peak was allowed to “float” during the iterative process; the best fit across the entire range of time-resolved experimental composite traces was found to be given when this third peak was located 120 mV positive in potential from the parent compound. A further effect, which occurred at longer

time, was the appearance of a peak at more negative potential than the parent or the 2,4-DNFB peak. The appearance of this peak was accompanied by a reduction in the height of the composite peak comprising the voltammetric responses of the parent, 2,4-DNFB, and the third peak.

A series of representative experimental SWV traces obtained at various time intervals from the same solution are shown in Figure 9. The features discussed above are illustrated; the solid line represents the experimental data, the dashed line represents the fit of the experimental data obtained by deconvolution, and the dotted lines represent the individual responses that make up the fit. By measuring the height of the individual component peaks, the relative contributions of the corresponding species to the voltammetric response could be assessed as a function of time, allowing the construction of a “reaction profile”, a representative example of which is depicted in Figure 10. Valuable mechanistic insights can be obtained through the careful interpretation of these reaction profiles, to which we return below.

3.5. Variation of Substrate Concentration. An experiment was performed to probe the effect of 2,4-DNCB concentration on the observed reaction profile during ultrasonic irradiation at intensity 25 W cm^{-2} ; apart from the reduced substrate concentration, the conditions were as described above. The amount of KF added was 2 g. The general form of the reaction profile obtained was analogous to that depicted in Figure 10. The 2,4-DNCB disappearance data is shown in Figure 11 along with that obtained using the higher substrate concentration of 10 mM. Initially, the consumption is fast with over 95% of the substrate being consumed in the first 1500 s of the reaction. Little consumption was observed subsequently. The “titration” effect observed in this experiment provides a rough estimate of the initial fluoride ion concentration as will be discussed more fully in the discussion section.

3.6. Sonication of Solutions of 2,4-DNCB and 2,4-DNFB in the Absence of KF. Solutions at a concentration of 10 mM of both 2,4-DNCB and 2,4-DNFB were prepared in DMF/0.1 M TBABF₄. The solutions were degassed with argon prior to sonication using an intensity of 50 W cm^{-2} for a period of 2 h during which the temperature was maintained at $85 \pm 1 \text{ }^\circ\text{C}$ by circulation of hot water. SWV traces were recorded every 15 min. The measured response was found to be unchanged in both cases, suggesting that neither the substrate employed or the intended product are susceptible to sonochemically induced reaction pathways in the reaction medium employed.

3.7. Sonication of 2,4-DNFB in the Presence of KF. Two grams of solid KF was added to a solution of 0.1 M TBABF₄ in DMF; the solution was sonicated using an intensity of 50 W cm^{-2} for 10 min. The ultrasound intensity was then reduced to 25 W cm^{-2} , and a quantity of 2,4-DNFB liquid was added by pipet to give a solution concentration of 10.0 mM. The solution was sonicated for 2 h, and SWV traces were gathered at regular intervals throughout.

Some broadening was observed on the positive side of the peak, and over time the height of the 2,4-DNFB peak was reduced by half, accompanied by the growth of a peak more negative in potential. The likely identity of this peak and the processes underlying its appearance are discussed below.

3.8 UV–Vis Data. Immediately upon addition of 2,4-DNCB stock solution to the presonicated suspension of KF in DMF/0.1 M TBABF₄, a color change was observed from clear to yellow. This yellow deepened to orange/red within 3–5 min of substrate addition; some further color change was discernible

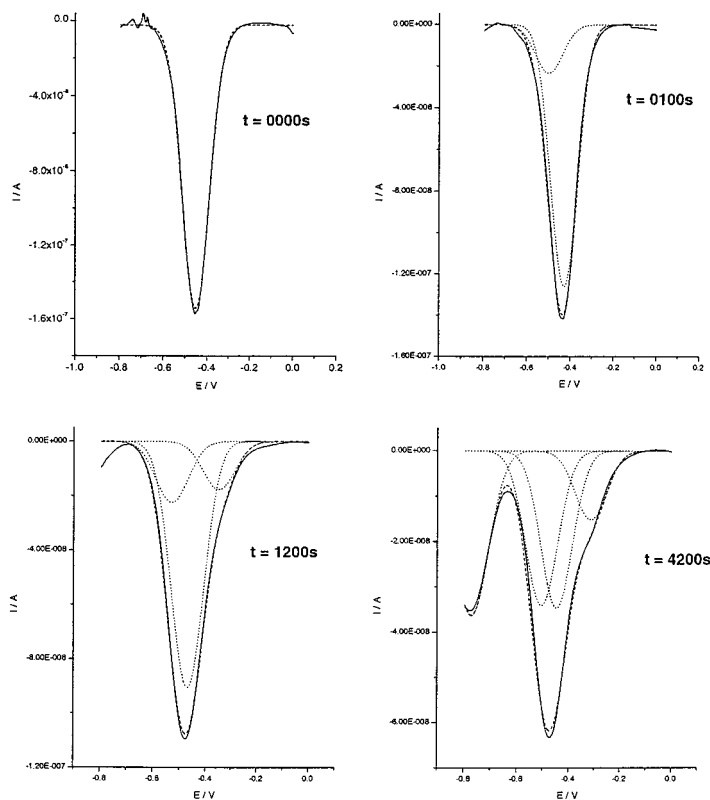


Figure 9. Square wave voltammograms obtained during the course of a typical HALEX reaction of 10 mM 2,4-DNCB with 2 g of KF in DMF 0.1 M/TBABF₄ at 85 °C: experimental data (solid); fit (dashed); contributions of individual components (dots). An ultrasound intensity of 50 W cm⁻² was employed.

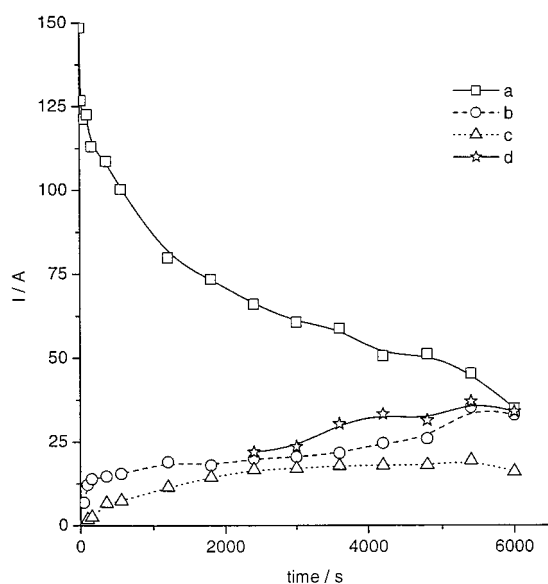


Figure 10. Reaction profile for the HALEX reaction of 10 mM 2,4-DNCB with 2 g of KF in DMF 0.1 M/TBABF₄ at 85 °C obtained through deconvolution of experimental SWV signal into individual components. An ultrasound intensity of 50 W cm⁻² was employed: (a) 2,4-DNCB; (b) 2,4-DNFB; (c) "component 3"; (d) "component 4".

by eye. To assess qualitatively this effect, samples were withdrawn from the reaction liquor at regular intervals and their absorption spectra were recorded after appropriate dilution. The effect of varying the added mass of KF was investigated in a series of experiments in which the higher ultrasound intensity of 50 W cm⁻² was employed. Two absorption maxima of approximately equal height were observed at wavelengths of 375 and 430 nm, and the height of both peaks increased with time.

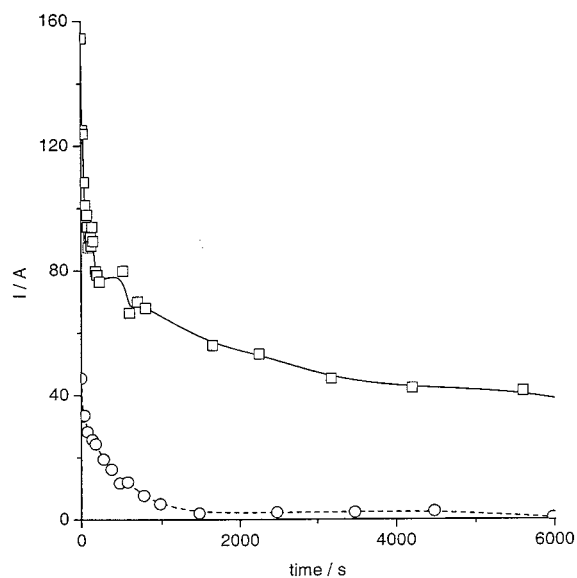


Figure 11. Decline of the current response for 2,4-DNCB during HALEX reaction with 2 g of KF in DMF 0.1 M/TBABF₄ at 85 °C. An ultrasound intensity of 25 W cm⁻² was employed. Starting concentrations of 2,4-DNCB were 3 mM (○) and 10 mM (□).

The observed absorption bands are consistent with the formation of the Meisenheimer complex [F-2,4-DNCB]⁻ as reported by Clark,³⁶ who observed absorption bands at 374 and 430 nm when solutions of 2,4-DNCB in various solvents were exposed to both homogeneous and heterogeneous sources of fluoride ion. This intermediate is shown, together with some of its major valence bond structures, in Scheme 2. From the data presented in ref 36, the extinction coefficient of [F-2,4-DNCB]⁻ was estimated as 87 500 M⁻¹ cm⁻¹, allowing the solution concentration of [F-2,4-DNCB]⁻ to be calculated from the

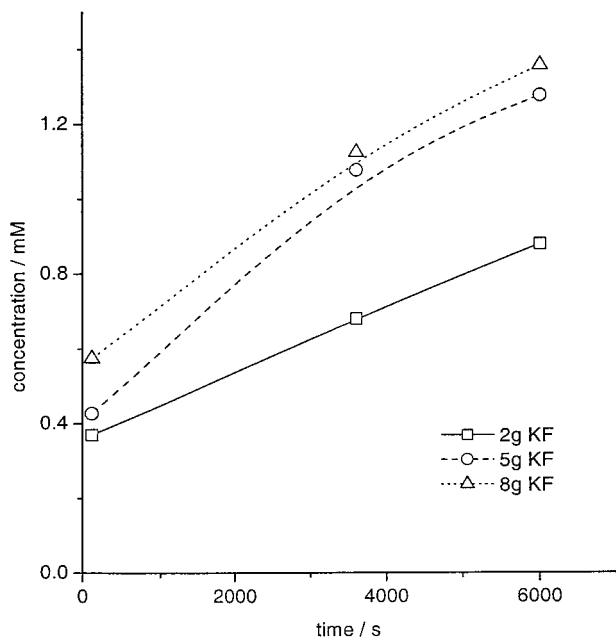
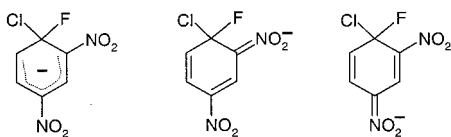


Figure 12. Concentration of the fluoro-Meisenheimer complex of 10 mM 2,4-DNCB present in solution as determined by UV–vis spectroscopy during the HALEX reaction of 2,4-DNCB with varying amounts of KF in DMF/0.1 M TBABF₄ at 85 °C. An ultrasound intensity of 50 W cm⁻² was employed.

SCHEME 2



absorption at 375 nm. Thus, Figure 12 shows the time evolution of [F-2,4-DNCB]⁻ concentration in the presence of various quantities of KF; the concentration increases with time up to a value of 1.4 mM.

4. Discussion

4.1 Explanation of Approach. In the kinetic treatment that follows, we confine our discussion to 2,4-DNCB disappearance because it is the consumption of 2,4-DNCB in the heterogeneous reaction that is of interest in determining the nature of the interfacial mechanism in operation. While the voltammetric response indicates the formation of products other than the intended halogen exchange product, the isolation of these products is beyond the scope of the current investigation. The likely identity of these species is discussed below. We initially limit our discussion to the reaction profiles obtained with an ultrasound intensity of 25 W cm⁻².

4.2. Implications of the Observed DNCB Disappearance Behavior. In all experiments employing 10 mM of substrate, the main feature of the reaction profile is an initial rapid disappearance of 2,4-DNCB over the first few hundred seconds followed by a far slower decrease at longer time. However, when the lower starting concentration of substrate of 3.0 mM was employed, all material was consumed rapidly (Figure 11), suggesting that the observed behavior could be accounted for by an initial phase of reaction with preexisting homogeneous fluoride anion followed by a phase in which the only available mechanism for 2,4-DNCB disappearance is reaction with fluoride ion following dissolution of solid KF. In the 3.0 mM experiment, all of the substrate reacted with fluoride ion already

in solution; hence, the second, slower phase of consumption was not observed.

4.3. Modeling the Disappearance of 2,4-DNCB. To examine the effect of coupled homogeneous and heterogeneous kinetics on the reaction profile, the following rate equations were considered: The first describes consumption of 2,4-DNCB by homogeneous reaction with fluoride according to the second-order rate constant k_{hom} .

$$\frac{dA}{dt} = -k_{\text{hom}}AB \quad (4.1)$$

where A is the concentration of 2,4-DNCB and B is the concentration of fluoride ion. The second describes consumption of fluoride ion by the homogeneous reaction above and production of fluoride ion by dissolution of KF, a process described by the Noyes–Whitney equation,³⁷

$$\frac{dB}{dt} = -k_{\text{hom}}AB + K_L(B_{\text{sat}} - B) \quad (4.2)$$

where B_{sat} is the saturation concentration of fluoride ion and K_L is an effective mass transport coefficient defined as

$$K_L = \frac{k_L a}{V} = \frac{Da}{\delta V} \quad (4.3)$$

where k_L is the mass transport coefficient, a is the surface area of dissolving solid, V is the volume of the solution, D is the diffusion coefficient, and δ is the diffusion layer thickness. We desire a solution for $A(t)$ and $B(t)$, the time-dependent concentrations of F⁻ and 2,4-DNCB, respectively, given eqs 4.1 and 4.2 above. We choose a fully implicit finite difference method with Richtmyer modification (FIRM algorithm) as reported by Feldberg^{38,39} to solve the defined problem.

The approximate solutions for $A(t)$ and $B(t)$ at times t_m will be labeled A_m and B_m . Also, because the flux of A and B is dominated by the second-order decay process (dA/dt and dB/dt are greatest at $t = 0$), we use a time function, t_m , where the time step increases geometrically to increase simulation speed:

$$\Delta t_m = \Delta t_0 \gamma^{m-1} = t_m - t_{m-1} \quad m = 1, 2, \dots, M \quad (4.4)$$

The mathematical derivation of this method is treated rigorously by Feldberg et al.³⁹ in previous literature. The time derivative of A is evaluated with the Richtmyer modification as

$$\left(\frac{dA}{dt}\right)_{m+1/2} \approx \frac{a_{2,A}}{(\partial t_m / \partial j)_{m+1/2}} = \frac{b_{2,A} + R_1 A_{m+1}}{(\partial t_m / \partial j)_{m+1/2}} \quad (4.5)$$

where

$$a_{2,A} = \sum_{j=1}^{j=j_{\text{level}}} R_j A_{m+2-j}$$

$$b_{2,A} = \sum_{j=2}^{j=j_{\text{level}}} R_j A_{m+2-j}$$

and R_j are a set of Richtmyer coefficients, specific to the number of concentration values used in the approximation, j_{level} . The differential $(\partial t_m / \partial j)_{m+1/2}$ for our chosen expanding time function is

$$(\partial t_m / \partial j)_{m+1/2} = -\frac{\Delta t \ln(\gamma) \gamma^{m+1/2}}{\gamma - 1} \quad (4.6)$$

Substitution of eq 4.3 into eq 4.4 yields

$$\frac{dB}{dt} = \frac{dA}{dt} + K_L(B_{\text{sat}} - B) \quad (4.7)$$

The fully implicit discretized form of eqs 4.1 and 4.5 become

$$\frac{b_{2,A} + R_1 A_{m+1}}{(\partial t_m / \partial j)_{m+1/2}} = -k_{\text{hom}} A_{m+1} B_{m+1} \quad (4.8)$$

and

$$\frac{b_{2,B} + R_1 B_{m+1}}{(\partial t_m / \partial j)_{m+1/2}} = \frac{b_{2,A} + R_1 A_{m+1}}{(\partial t_m / \partial j)_{m+1/2}} + K_L(B_{\text{sat}} - B_{m+1}) \quad (4.9)$$

Substituting the isolated solution for B_{m+1} from eq 4.7

$$B_{m+1} = -\frac{R_1 A_{m+1} + b_{2,A}}{k_{\text{hom}}(\partial t_m / \partial j)_{m+1/2} A_{m+1}} \quad (4.10)$$

into eq 4.8 results in a solvable quadratic equation in A_{m+1} .

$$0 = A_{m+1}^2(-R_1) + A_{m+1} \left(b_{2,B} - b_{2,A} - K_L(\partial t_m / \partial j)_{m+1/2} B_{\text{sat}} - \frac{R_1(R_1 + K_L(\partial t_m / \partial j)_{m+1/2})}{k_{\text{hom}}(\partial t_m / \partial j)_{m+1/2}} \right) - \frac{b_{2,A}}{k_{\text{hom}}(\partial t_m / \partial j)_{m+1/2}} (R_1 + K_L(\partial t_m / \partial j)_{m+1/2}) \quad (4.11)$$

Equations 4.10 and 4.11 specify an iterative method for the solutions A_{m+1} and B_{m+1} . The startup protocol involves setting $A_0 = A_{-1} = A_{-2} \dots = A_{2-j_{\text{level}}}$ and $B_0 = B_{-1} = B_{-2} \dots = B_{2-j_{\text{level}}}$. The use of an expanding time step, several Richtmyer levels, and fully implicit formulation of the problem allows an iterative solution of high accuracy to be computed quickly on contemporary computers. This allows the analysis of the experimental data to be achieved with an appropriate multidimensional function minimization algorithm, rather than a working (hyper)-surface interpolation method.^{40,41}

4.4. Computation. The data analysis (Simplex method) and visualization were written for and performed using IDL 5.0⁴² on a Silicon Graphics Indigo 2 workstation. The solution to eqs 4.10 and 4.11 was written in C++ as an external program, which was then called from IDL using the SPAWN function. In all simulations, the following parameters were used: $j_{\text{level}} = 6$; $\gamma = 1.005$; $\Delta t_0 = 4.0$ s; $M = 500$; $B_0 = 10^{-5}$; $f_{\text{tol}} = 10^{-4}$.

4.5 Analysis. *4.5.1. Method.* Inspection of the kinetic eqs 4.1 and 4.2 shows that the solutions, $A(t)$ and $B(t)$, are functions of the variables, k_{hom} , K_L , B_0 , A_0 , and B_{sat} . The experimental setup demands that A_0 takes a known value. Also to simplify the system, by setting $B_0 = B_{\text{sat}}$, which is a reasonable assumption because all solutions were sonicated for 10 min at reaction temperature prior to substrate addition, we reduce the multidimensional search to three variables. The search involves locating the global minimum in the error between experimental and numerically calculated values of $A(t)$. The error calculated as the mean absolute deviation (MAD) is formally defined as

$$\text{MAD} = \frac{1}{n} \sum_{i=1}^n |A_{\text{exp}}(t_i) - A_{\text{theory}}(t_i)| \quad (4.12)$$

where n is the number of points in the experimental data set and $A_{\text{exp}}(t_i)$ and $A_{\text{theory}}(t_i)$ are the experimentally and theoretically

TABLE 1: Results of Simulation for the HALEX Reaction of 10 mM 2,4-DNCB with 2 g of KF in DMF/0.1 M TBABF₄ at 85 °C^a

[KF], g	k_{hom} , mol ⁻¹ cm ³ s ⁻¹	K_L , s ⁻¹	B_{sat} , mM	MAD, mM
1	385	2.50×10^{-5}	5.99×10^{-6}	5.61×10^{-7}
2	830	3.45×10^{-5}	6.40×10^{-6}	5.93×10^{-7}
5	566	7.30×10^{-5}	6.63×10^{-6}	3.96×10^{-7}
8	776	9.55×10^{-5}	6.93×10^{-6}	2.95×10^{-7}

^a An ultrasound intensity of 25 W cm⁻² was employed.

calculated values of the concentration solution $A(t)$ at the experimental time point t_i . In practice, linear interpolation was used to determine the value of $A_{\text{theory}}(t_i)$ given t_i and a vector of solutions, A_m . The algorithm used to search the three-dimensional variable space for a minimum in MAD was the downhill simplex method.²⁸ This algorithm uses a selection of transformations on an n -dimensional simplex formed from $n + 1$ search vectors (k^j , K_L^i , B_{sat}^i , $i = 1, \dots, n + 1$). When the fractional difference between the highest and lowest function values of the simplex drops below a predefined tolerance f_{tol} , the search vector yielding the lowest function value is considered optimum and the algorithm terminates. It is best to restart the algorithm at this position to verify that the minimum is global and not local.

4.5.2. Results. Initial results were gathered for the four experiments in which sonication at a level of 25 W cm⁻² was employed. The initial concentration of 2,4-DNCB was 10 mM, and the weights of added KF were 1, 2, 5, and 8 g.

The optimum values found by the simplex method are tabulated in Table 1, while plots of the corresponding fit between experimental and theoretical data are shown Figure 13. As can be seen from the data, optimized B_{sat} and k_{hom} values are consistent across experiments. The mean value for the homogeneous rate constant for the reaction of 2,4-DNCB with fluoride ion is 640 ± 250 mol⁻¹ cm³ s⁻¹, and the mean value for the saturation concentration of fluoride ion is $(6.5 \pm 0.5) \times 10^{-6}$ mol cm⁻³.

The consistency of the homogeneous rate constants provides strong evidence that homogeneous reaction with preexisting fluoride ion is the initial mechanism for 2,4-DNCB disappearance. Furthermore, this mechanism is in operation across the entire range of solid–liquid compositions studied.

The values obtained for the saturated fluoride ion concentration are independent of the amount of solid KF initially present. This provides compelling evidence that the 10 min presonation period does indeed saturate the solution with fluoride ion and that the method employed gives a consistent and accurate indirect measure of the solution fluoride concentration.

The K_L values exhibit a linear trend with added KF (Figure 14). K_L is a composite of the mass-transfer coefficient and the ratio of the KF surface area to reactor volume. Because the value of the mass-transfer coefficient is determined by the operative convective regime and the diffusion coefficient of the species being transferred, it would be expected to be constant for a given chemical species and ultrasound intensity. The surface area of KF available for dissolution is directly proportional to the mass of KF; hence, the observed linear increase in rate with increasing solid–liquid ratio demonstrates that the reaction rate is *dissolution-rate-limited* at long time, although, of course, the site of the chemical reaction remains homogeneous.

4.6. Ultrasound Effects. The above discussion clearly demonstrates the physical meaning of the observed concentration profiles in terms of coupled homogeneous and heterogeneous kinetics, showing how the experimental data could be accounted

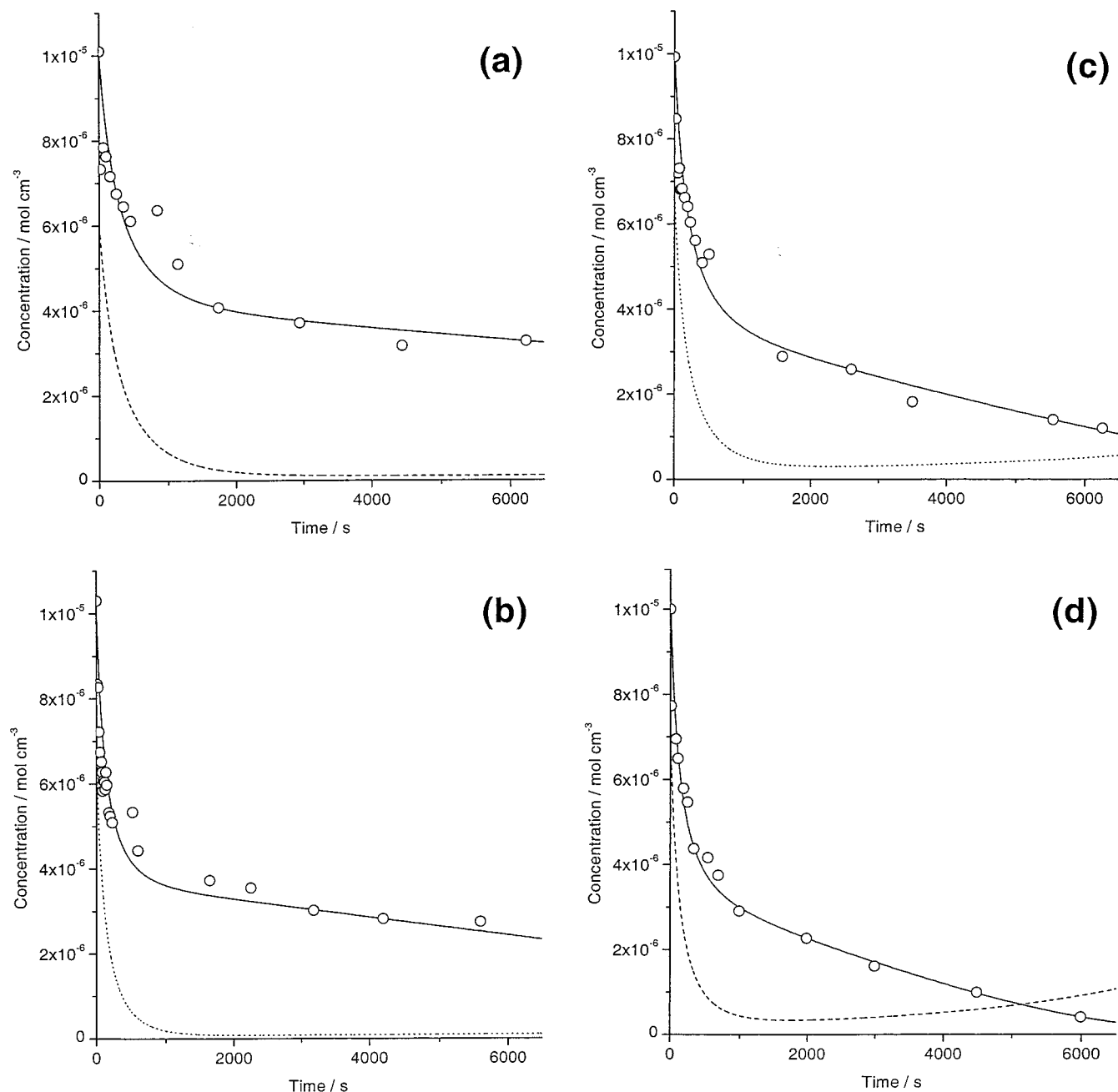


Figure 13. Comparison of experimentally measured (○) and modeled (solid line) 2,4-DNCB concentration profiles for the HALEX reaction of 10 mM 2,4-DNCB with varying amounts of KF in DMF/0.1 M TBABF₄ at 85 °C. The modeled fluoride ion concentration is also shown (dotted line). An ultrasound intensity of 25 W cm⁻² was employed. Amounts of KF were (a) 1 g, (b) 2 g, (c) 5 g, and (d) 8 g.

for in all cases using the same homogeneous rate constant and the saturated fluoride ion concentration while allowing the K_L term to vary. The K_L term was found to scale linearly with the mass of KF added to the system (Figure 14), implying that a dissolution rate constant could be estimated using eq 4.3; however, in practice, the actual surface area of KF is unknown. When the higher ultrasound intensity of 50 W cm⁻² was utilized, the results were in good agreement with those obtained using the lower ultrasound intensity of 25 W cm⁻².

Two conclusions can be drawn from comparison of the 2,4-DNCB disappearance profiles obtained using different levels of ultrasonic irradiation: First, as demonstrated by the agreement between the data obtained using 50 W cm⁻² and that obtained using 25 W cm⁻², there is no significant effect of ultrasound in accelerating the disappearance of 2,4-DNCB. From this it follows that there is no significant effect of ultrasound in

promoting the dissolution of KF, a conclusion which may at first seem counterintuitive and at odds with a previous study in which the flux of material from an insonated disk of solid material was found to increase slightly with increasing ultrasound intensity.⁴³ It is, however, readily explicable when the experimental configuration is carefully considered. The primary function of the ultrasonic irradiation in this current study is to keep the KF particles suspended; they circulate around the reaction vessel and as such are only exposed periodically to the regime of high-intensity cavitation and consequent micro-jetting, which occurs only immediately adjacent to the horn tip. Hence, mass transport from the solid surface to bulk solution occurs not through the intensely thinned diffusion layer of a directly insonated disk but through a much larger diffusion layer, primarily enforced by the shear forces exerted by the particle as it moves through the solution and through bulk convection.

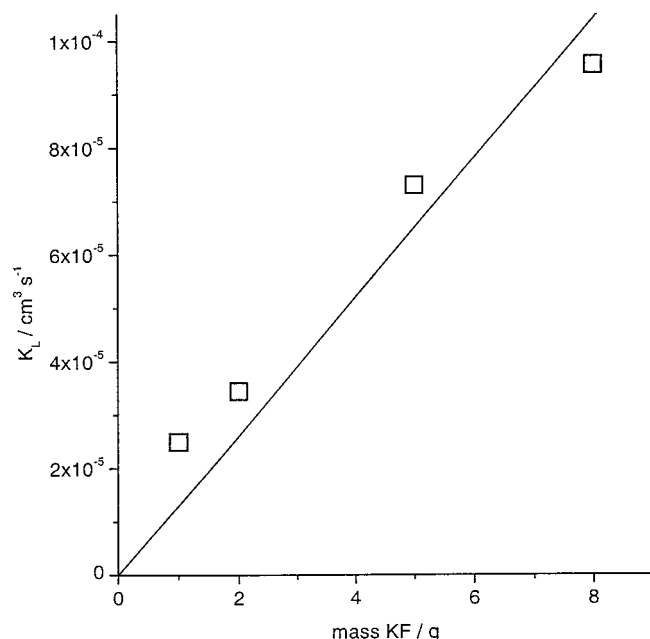
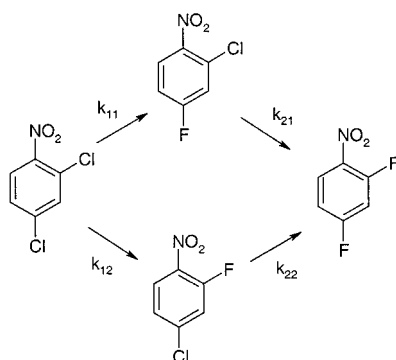


Figure 14. Simulated effective mass transfer coefficient, K_L , for the dissolution of KF into DMF/0.1 M TBABF₄ at 85 °C as a function of the initial mass of KF. An ultrasound intensity of 25 W cm⁻² was employed.

SCHEME 3



Hence, there is no significant effect of ultrasound intensity on solid dissolution rates in a dispersed system.

The second conclusion that can be drawn is a more general conclusion relating to the applicability of microelectrode detection techniques to heterogeneous systems. By virtue of their small size, microelectrodes sample a very small volume of solution. In truly homogeneous solutions, this yields a true measure of bulk solution concentration. In heterogeneous systems, however, the composition of the small volume sampled, and hence the current response, may differ substantially depending on the precise location of the electrode. Microelectrodes have been successfully applied to the *in situ* measurement of trace elements in sediment porewater,¹⁷ local oxygen concentrations in clay soils¹⁸ and biofilms,¹⁹ and mixing-induced heterogeneities in continuously stirred tank reactors.²⁰ In an *intrinsically heterogeneous* system, such as the subject of this current study, the observed microelectrode response is strongly dependent on the solution conditions local to the electrode, as is clearly demonstrated by the highly scattered and nonsystematic results obtained in the mechanically stirred case. Indeed, that systematic and reproducible results were obtained in the experiments in which ultrasonically induced mixing was employed is a strong argument for the application of power ultrasound to *intrinsically heterogeneous* systems in which it

is desired to obtain meaningful and representative measurements using microelectrode techniques.

Recent investigations into the mechanism of heterogeneous HALEX reactions have focused on the fluorination of 2,4-dichloronitrobenzene using solid KF and have yielded contradictory conclusions. We now consider this contradiction in the light of the results of our current investigation into 2,4-DNCB. Study of the reaction using a dispersed powder reactor¹⁴ over a wide concentration range found that the observed rate could be homogeneous-reaction-rate-limited, dissolution-rate-limited, or operating in a mixed kinetic regime in which both processes have an influence on the observed rate. An expression was derived that was identical to that resulting from our own treatment under the assumption of steady-state conditions ($dB/dt = 0$):

$$q = \frac{VB_{\text{sat}}}{\frac{1}{k_{\text{hom}}A} + \frac{V}{k_L a}} \quad (4.13)$$

where q is the observed rate in mol s⁻¹ and V is the reactor volume. Importantly, this current study applies also to non-steady-state conditions and provides an indirect measurement of the time-dependent actual fluoride concentration.

Other studies have concluded that the fluorination of 2,4-dichloronitrobenzene using solid KF is a true surface reaction, the rate of which is limited by the formation of a surface complex. Smyth⁵ considers both the phase-transfer mechanism, in which the reaction occurs homogeneously following dissolution of KF, and the interfacial mechanism, in which the rate-determining step is a complex formed on the solid surface; the phase-transfer mechanism in this case is dismissed because of the calculation of a large Hammett reaction constant ($\rho = +6.4$) and the observation that the rate of disappearance of the starting material is proportional to the stirring speed. The fluorination of 2,4-dichloronitrobenzene proceeds via two competing mechanisms; ortho- followed by para-substitution is favored, but para-followed by ortho-substitution is a competing pathway to the difluorinated product (Scheme 3). Langlois et al.² consider the observed relative rates of ortho- and para-substitution in both the first and second fluorination step (k_{11}/k_{12} and k_{22}/k_{21} , respectively) and the fact that they depend on the source of the KF before concluding that homogeneous reaction must be ruled out, favoring instead the mechanism proposed by Sasson⁴⁴ for the heterogeneous fluorination of *n*-octyl chloride, in which the reaction proceeds in a border phase at the solid-liquid interface consisting mostly of solvent but with a higher concentration of phase-transfer catalyst than that found in bulk solution.

The results of our current study provide compelling evidence for homogeneous reaction following dissolution of KF; indeed, it is even possible to discern the point at which kinetic control switches from homogeneous reaction to dissolution-rate-limited reaction and hence to provide an elegant extension of the treatment presented in ref 14. It should however be noted that the results of Smyth and Langlois are not necessarily inconsistent with those presented here, because the observation that reaction rate is proportional to stirring speed does not necessarily imply that the reaction is occurring at an interface; a homogeneous reaction limited by dissolution rate of one or more reactants would display the same behavior. The observation of the large Hammett reaction constant shows that the rate is strongly influenced by substituent effects; this was interpreted as proof that KF dissolution was not the rate-determining step; however, a large Hammett reaction constant is exactly what would be

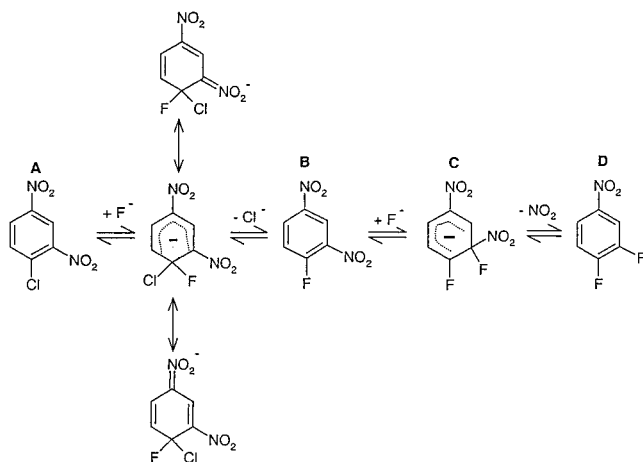


Figure 15. Proposed scheme for the fluorination of 2,4-dinitrochlorobenzene. The voltammetrically visible species are denoted **A**, **B**, **C**, and **D**.

anticipated when the reaction occurs homogeneously following KF dissolution. Furthermore, perusal of the data presented in ref 2 shows that the ratios k_{11}/k_{12} and k_{22}/k_{21} vary with the source of KF and the presence of phase-transfer catalysts. However, the variation is surprisingly small ($k_{11}/k_{12} = 2.9$ (SD = 0.5) and $k_{22}/k_{21} = 1.0$ (SD = 0.5) ($n = 10$)) and hence probably argues in favor of the homogeneous-reaction hypothesis.

The observation by UV–vis spectroscopy of the Meisenheimer complex $[F\text{-}2,4\text{-DNCB}]^-$ in solution adds yet more weight to the hypothesis of homogeneous reaction. If any ternary complex was formed on the surface between the tetrabutylammonium cation, the substrate, and the ionic solid, it would remain there until the fluorinated product was formed, rather than desorbing as an intermediate complex. This observation is highly relevant as it confirms that the reaction does indeed proceed via a two-step mechanism with a Meisenheimer intermediate; it has been postulated that 2,4-DNCB may react with other nucleophiles via a multistep mechanism within the solvent cage that has as its first step a single electron transfer between the reactants.⁴⁵

From the analysis above, it is clear that the mechanistic interrogation of systems in which the overall kinetics are determined by both dissolution and homogeneous reaction, such as the heterogeneous HALEX reaction considered here, presents a significant challenge. This is because the same system can exhibit diverse kinetic behavior under different conditions, behaving on one hand as a dissolution-rate-controlled process and on the other as a homogeneous chemical process as described in ref 14. The experiment presented here is unusual in that *both* regimes are visible in the same experiment: initially, homogeneous reaction dominates the observed kinetics as the presaturated solution is stripped of fluoride ion; at longer time, the observed kinetics are controlled by the rate of KF dissolution.

4.7. Assignment of SWV Peaks. Although only the 2,4-DNCB data have been used in the analysis for reasons stated above, the appearance and position of the other peaks can be rationalized according to the scheme presented in Figure 15. The initial peak can unquestionably be assigned to 2,4-DNCB (**A**), and the fact that the disappearance of this peak is accompanied by the growth of a peak at a potential corresponding to 2,4-DNFB (**B**) makes the assignment of this peak definite. Furthermore, we speculate that the third peak, occurring 120 mV positive in potential of 2,4-DNCB could be attributed to the Meisenheimer intermediate of a second fluorination step (**C**), in this case a fluorodenitration as described by Clark.⁶ This is

plausible as a fluorinated nitroalkane would be expected to have a more positive reduction potential than the fluorinated nitroaromatic from which it was formed. We speculate that the fourth peak, centered around -0.7 V vs Ag, is the product of this fluorodenitration reaction, 3,4-difluoronitrobenzene (**D**). There are no data in the literature concerning the reduction potential of this compound, but it might reasonably be expected to be more negative in potential than the monofluorinated compound from which it was formed. The only species unaccounted for in the proposed scheme is the Meisenheimer complex $[F\text{-}2,4\text{-DNCB}]^-$, which we suggest might likely be voltammetrically invisible in the potential scan range studied.

5. Conclusions

The HALEX reaction of 2,4-dichloronitrobenzene with potassium fluoride in the presence of tetrabutylammonium salts in dimethylformamide has been studied employing an electrochemical detection methodology based upon the use of square wave voltammetry. The problem of overlapping signals was resolved by curve fitting. The results presented show that the kinetics of the HALEX reaction studied exhibit diverse kinetic behavior under different conditions, behaving on one hand as a dissolution-rate-controlled process and on the other as a homogeneous chemical process. The experiment presented here is unusual in that *both* regimes are visible in the same experiment: initially homogeneous reaction dominates the observed kinetics as the presaturated solution is stripped of fluoride ion; at longer time, the observed kinetics are controlled by the rate of KF dissolution. Ultrasound was found not to significantly enhance the rate of the reaction in the intensity range studied.

The theory used to interpret the experimental results is in principle applicable to all chemical systems involving mixed kinetic regimes. Furthermore, the utility of microelectrodes for obtaining simple quantifiable voltammetric responses from compounds of which the macroelectrode responses are complicated by chemical followup steps has been demonstrated. Ultrasonically induced mixing has been shown to facilitate reproducible microelectrode responses in intrinsically heterogeneous systems.

Acknowledgment. We thank the EPSRC for support for G.M. and B.A.B. and Avecia for funding through a CASE studentship for G.M.

References and Notes

- (1) Adams, D. J.; Clark, J. H. *Chem. Soc. Rev.* **1999**, 28, 225.
- (2) Langlois, B.; Gilbert, L.; Forat, G. *Ind. Chem. Libr.* **1996**, 8, 244.
- (3) Ishikawa, N.; Kitazume, T.; Yamazaki, T.; Mochida, Y.; Tatsuno, T. *Chem. Lett.* **1981**, 761.
- (4) Kimura, Y.; Suzuki, H. *Tetrahedron Lett.* **1989**, 30, 1271.
- (5) Smyth, T. P.; Carey, A.; Hodnett, B. K. *Tetrahedron* **1995**, 51, 6363.
- (6) Clark, J. H.; Cork, D. G.; Robertson, M. S. *Chem. Lett.* **1983**, 1145.
- (7) Clark, J. H.; Hyde, A. J.; Smith, D. K. *J. Chem. Soc., Chem. Commun.* **1986**, 791.
- (8) Miyajima, F.; Iijima, T.; Tomoi, M.; Kimura, Y. *React. Funct. Polym.* **2000**, 43, 315.
- (9) Clark, J. H.; Smith, D. K. *Tetrahedron Lett.* **1985**, 26, 2233.
- (10) Boechat, N.; Clark, J. H. *J. Chem. Soc., Chem. Commun.* **1993**, 921.
- (11) Esikova, I. A.; Yufit, S. S. *J. Phys. Org. Chem.* **1991**, 4, 149.
- (12) Esikova, I. A.; Yufit, S. S. *J. Phys. Org. Chem.* **1991**, 4, 341.
- (13) Yufit, S. S.; Esikova, I. A. *J. Phys. Org. Chem.* **1991**, 4, 336.
- (14) Atherton, J. H. *Res. Chem. Kinet.* **1994**, 2, 193.
- (15) Sanger, F. *Biochem. J.* **1949**, 45, 563.
- (16) Brett, C. M. A.; Brett, A. M. O. *Electrochemistry: principles, methods, and applications*; Oxford University Press: Oxford, U.K., 1993.

- (17) Luther, G. W., III.; Brendel, P. J.; Lewis, B. L.; Sundby, B.; Lefrancois, L.; Silverberg, N.; Nuzzio, D. B. *Limnol. Oceanogr.* **1998**, *43*, 325.
- (18) Bakker, D. M.; Bronswijk, J. J. B. *Soil Sci.* **1993**, *155*, 309.
- (19) Rasmussen, K.; Lewandowski, Z. *Biotechnol. Bioeng.* **1998**, *59*, 302.
- (20) Menzinger, M.; Dutt, A. K. *React. Kinet. Catal. Lett.* **1990**, *42*, 419.
- (21) Lindley, J.; Mason, T. J. *Chem. Soc. Rev.* **1987**, *16*, 275.
- (22) Davidson, R. S.; Safdar, A.; Spencer, J. D.; Robinson, B. *Ultrasonics* **1987**, *25*, 35.
- (23) Hagenson, L. C.; Naik, S. D.; Doraiswamy, L. K. *Chem. Eng. Sci.* **1994**, *49*, 4787.
- (24) Ratoarinoro, N.; Wilhelm, A. M.; Berlan, J.; Delmas, H. *Chem. Eng. J. Biochem. Eng. J.* **1992**, *50*, 27.
- (25) Naik, S. D.; Doraiswamy, L. K. *Am. Inst. Chem. Eng. J.* **1998**, *44*, 612.
- (26) Cardwell, T. J.; Mocak, J.; Santos, J. H.; Bond, A. M. *Analyst* **1996**, *121*, 357.
- (27) Mason, T. J.; Lorimer, J. P.; Bates, D. M. *Ultrasonics* **1992**, *30*, 40.
- (28) Press, W. H.; Vetterling, W. T. *Numerical recipes in C: the art of scientific computing*, 2nd ed.; Cambridge University Press: Cambridge, U.K., 1992.
- (29) Gallardo, I.; Guirado, G.; Marquet, J. *J. Electroanal. Chem.* **2000**, *488*, 64.
- (30) Moressi, M. B.; Fernandez, H. *J. Electroanal. Chem.* **1994**, *369*, 153.
- (31) Bard, A. J.; Faulkner, L. R. *Electrochemical methods: fundamentals and applications*; Wiley: New York, Chichester, U.K., 1980.
- (32) Wilke, C. R.; Chang, P. *Am. Inst. Chem. Eng. J.* **1955**, *1*, 264.
- (33) Bard, A. J.; Lund, H. *Encyclopedia of electrochemistry of the elements*; M. Dekker: New York, 1973.
- (34) Brookes, B. A.; Ball, J. C.; Compton, R. G. *J. Phys. Chem. B* **1999**, *103*, 5289.
- (35) Aoki, K.; Maeda, K.; Osteryoung, J. *J. Electroanal. Chem. Interfacial Electrochem.* **1989**, *272*, 17.
- (36) Clark, J. H.; Robertson, M. S.; Smith, D. K.; Cook, A.; Streich, C. *J. Fluorine Chem.* **1985**, *28*, 161.
- (37) Mall, S.; Buckton, G.; Rawlins, D. A. *Int. J. Pharm.* **1996**, *131*, 41.
- (38) Feldberg, S. W.; Goldstein, C. I. *J. Electroanal. Chem.* **1995**, *397*, 1.
- (39) Mocak, J.; Feldberg, S. W. *J. Electroanal. Chem.* **1994**, *378*, 31.
- (40) Alden, J. A.; Compton, R. G. *J. Phys. Chem. B* **1997**, *101*, 9741.
- (41) Brookes, B. A.; Lawrence, N. S.; Compton, R. G. *J. Phys. Chem. B* **2000**, *104*, 11258.
- (42) Floating point systems. <http://www.floating.co.uk/idl/> (accessed Nov 2001).
- (43) Macfie, G.; Compton, R. G. *J. Electroanal. Chem.* **2001**, *503*, 125.
- (44) Dermeik, S.; Sasson, Y. *J. Org. Chem.* **1985**, *50*, 879.
- (45) Grossi, L.; Strazzari, S. *J. Chem. Soc., Perkin Trans. 2* **1999**, 2141.